Check for updates

# Model-based redatuming of seismic data: An inverse-filter approach

Thomas Planès[1], Roel Snieder[2], and Satyan Singh[2]

## ABSTRACT

Standard model-based redatuming techniques allow focusing of the direct waves at the new datum, but the focus can be degraded because of surface multiples and internal multiples in the overburden. We demonstrate that if the medium above the redatuming level is known, these multiples can be correctly handled. We compute the exact focusing functions, free of multiples, using an inverse-filter approach. These focusing functions create downward-radiating and upward-radiating virtual sources at the new datum. The surface responses to these virtual sources are then used to compute the objective redatumed data set through multidimensional deconvolution. The redatumed data set corresponds to a virtual acquisition made at the new datum and for which the imprint of the overburden is completely removed. We test the technique on 2D acoustic synthetic examples corresponding to a seismic context and an acoustic nondestructive testing context.

## INTRODUCTION

Redatuming seismic data corresponds to virtually moving the sources and receivers from the original acquisition level to a new depth level, also called the new datum. This process can be used when the original acquisition grid is inadequate for imaging purposes, such as in cases of rugged topography, irregular spatial sampling, remoteness from the target, etc.

When buried sensors are available at the new datum (e.g., in a deviated well), creating virtual sources can be achieved based on the data only, without any prior knowledge of the medium. Processing techniques have been developed for this purpose and fall into the category of correlation-based redatuming (Bakulin and Calvert, 2005; Schuster and Zhou, 2006). In particular, the interferometry by multidimensional deconvolution procedure can be applied to fully cancel the effect of the overburden, provided that the upgoing and downgoing waves at the redatuming level are known (Wapenaar et al., 2008; Wapenaar and van der Neut, 2010; van der Neut et al., 2011a, 2011b).

When buried sensors are not available, model-based redatuming relies on applying corrections to the original data set based on some prior knowledge of the overburden, i.e., some knowledge of the medium parameters between the original datum and the new datum. The standard approach relies on modeling the propagation of the direct waves between the surface and the positions of the virtual sources/receivers and in applying extrapolation operators to the data (Berryhill, 1979; Shtivelman and Canning, 1988). These extrapolation operators apply appropriate time shifts and amplitude corrections to each trace. This approach only requires a macrovelocity model of the overburden as prior information. If no assumption is made about the overburden, it is also possible to estimate time shifts by crosscorrelating neighboring traces. Explicitly applying those time shifts to the traces is known as static correction. Static correction was the first redatuming-like technique to be developed in seismic exploration (Hileman et al., 1968; Taner et al., 1974; Rothman, 1986).

The standard model-based redatuming methods can successfully focus the direct waves at the new datum, but they do not account for surface multiples and internal multiples in the overburden. These multiples can generate ghost arrivals in the redatumed data set and thus ghost reflectors in the subsequent images. In the field of acoustics, a similar problem of imperfect focusing has led to the development of the spatiotemporal inverse-filter technique (Tanter et al., 2001). With a single-sided source distribution, this technique aims to focus acoustic wavefields beyond complicated layers for medical imaging and nondestructive-testing purposes (Aubry et al., 2001). It requires the acquisition of a baseline data set (a transmission matrix), for which the "overburden" is extracted from the rest of the medium. With sources on one side and receivers on the other

[1]Center for Wave Phenomena, Colorado School of Mines, Golden, Colorado, USA and University of Geneva, Department of Earth Sciences, Genève, Switzerland. E-mail: thomas.planes@unige.ch.
[2]Center for Wave Phenomena, Colorado School of Mines, Golden, Colorado, USA. E-mail: rsnieder@mines.edu; s.singh@ed.ac.uk.

side of the overburden, the transmission matrix is acquired, and focusing functions are built through an inversion procedure.

In a seismic context, a physical acquisition of such a baseline is not possible. However, if one has a good knowledge of the medium parameters in the overburden, the transmission matrix can be estimated with numerical simulations of wave propagation through the overburden. This is the approach that we use here to compute the focusing functions.

In contrast, the recently developed Marchenko imaging procedure aims to iteratively infer these same focusing functions, only using reflected waves recorded at the surface and a macrovelocity model as prior information (Rose, 2002; Wapenaar et al., 2013; Broggini et al., 2014; da Costa Filho et al., 2014; van der Neut et al., 2015). The approach that we propose here thus requires more prior information than the Marchenko method, but it can provide in turn a more direct way to compute these focusing functions.

The focusing functions are then used to compute the surface responses to upward-radiating and downward-radiating virtual sources at the new datum. Finally, the imprint of the overburden is fully removed through multidimensional deconvolution. Our work is related to the "rigorous redatuming" method developed by Mulder (2005), which requires similar assumptions and aims at the same objective. However, we follow a different approach based on the reciprocity theorems (Appendix A), and our formalism involves one less inversion step in the redatuming procedure. The differences between the approach of Mulder (2005) and our approach are detailed in the "Discussion" section. We also present a heuristic connection with the previously developed inverse-filter technique and Marchenko imaging method.

The formal derivation of the redatuming equations, based on Rayleigh's reciprocity theorem, is presented in Appendix B. In the main text, we provide a heuristic graphics-based derivation that relies on a matrix formalism. We then demonstrate the method on two synthetic data sets: one corresponding to a seismic context and the other corresponding to an acoustic nondestructive-testing context (small-scale and reflective side boundaries). In both cases, we retrieve the redatumed Green's functions for which the imprint of the overburden is removed.

## THEORY

We consider a 2D acoustic medium with variable density $\rho(\mathbf{r})$ and compression modulus $\kappa(\mathbf{r})$. The frequency-domain wave equation for the pressure $p(\mathbf{r}, \omega)$ reads

$$\rho(\mathbf{r})\nabla.\left[\frac{1}{\rho(\mathbf{r})}\nabla p(\mathbf{r},\omega)\right] + \frac{\omega^2}{c^2(\mathbf{r})}p(\mathbf{r},\omega) = f(\mathbf{r},\omega), \quad (1)$$

where $\omega$ is the angular frequency, $c(\mathbf{r}) = \sqrt{\kappa/\rho}$ is the medium's velocity, and $f(\mathbf{r}, \omega)$ is an arbitrary source term. We define the Green's function $g(\mathbf{r}, \mathbf{r_s}, \omega)$ as the solution of this wave equation for a monopole Dirac source term at $\mathbf{r_s}$; i.e.,

$$\nabla.\left[\frac{1}{\rho(\mathbf{r})}\nabla g(\mathbf{r},\mathbf{r_s})\right] + \frac{\omega^2}{\kappa(\mathbf{r})}g(\mathbf{r},\mathbf{r_s}) = \delta(\mathbf{r}-\mathbf{r_s}), \quad (2)$$

where the frequency dependency of the Green's functions is made implicit from now on. Note that the density has been included in the source term, so that the Green's function is the solution of the wave equation (equation 1) with a source term $f(\mathbf{r},\omega) = \rho(\mathbf{r})\delta(\mathbf{r}-\mathbf{r_s})$. This definition of the Green's function ensures that the source-receiver reciprocity property is satisfied (Rayleigh, 1878; Snieder and van Wijk, 2015, expression 18.64); i.e,

$$g(\mathbf{r_1},\mathbf{r_2}) = g(\mathbf{r_2},\mathbf{r_1}). \quad (3)$$

In the absence of horizontally propagating waves, the Green's function can be decomposed at the receiver level into an upgoing part and a downgoing part as

$$g(\mathbf{r},\mathbf{r_s}) = g^{+,p}(\mathbf{r},\mathbf{r_s}) + g^{-,p}(\mathbf{r},\mathbf{r_s}), \quad (4)$$

where $g^{+,p}(\mathbf{r},\mathbf{r_s})$ represents the downgoing pressure wavefield at $\mathbf{r}$ (superscript $+$) for an impulsive pressure source at $\mathbf{r_s}$ (superscript $p$) and where $g^{-,p}(\mathbf{r},\mathbf{r_s})$ represents the upgoing pressure wavefield at $\mathbf{r}$ (superscript $-$) for an impulsive pressure source at $\mathbf{r_s}$ (superscript $p$). By analogy with the reciprocity relation (equation 3), we establish the conventions

$$g^{p,-}(\mathbf{r_1},\mathbf{r_2}) \equiv g^{+,p}(\mathbf{r_2},\mathbf{r_1}),$$
$$g^{p,+}(\mathbf{r_1},\mathbf{r_2}) \equiv g^{-,p}(\mathbf{r_2},\mathbf{r_1}), \quad (5)$$

where $g^{p,+}(\mathbf{r_1},\mathbf{r_2})$ is seen as the full pressure wavefield at $\mathbf{r_1}$ (superscript $p$) for a downward-radiating pressure source at $\mathbf{r_2}$ (superscript $+$) and where $g^{p,-}(\mathbf{r_1},\mathbf{r_2})$ is seen as the full-pressure wavefield at $\mathbf{r_1}$ (superscript $p$) for an upward-radiating pressure source at $\mathbf{r_2}$ (superscript $-$). This convention is used to help the heuristic understanding of the redatuming procedure, and the two notations are always interchangeable.

We consider $N$ sources and $N$ receivers at coinciding locations just below the free surface, whose positions are described by the coordinate $x^0$ (Figure 1a). We define the $N \times N$ reflection matrix $\mathbf{R}$ of the full medium as $\{R\}_{ij} = g(x_i^0, x_j^0, \omega)$. It contains the responses from each source position $x_j^0$ to each receiver position $x_i^0$, and it corresponds to a reflection data set acquired at the free surface.

Our objective is to transform the initial reflection data set $\mathbf{R}$ into a virtual reflection data set $\mathbf{R_1^L}$, corresponding to virtual sources and receivers located at depth $z_1$ and for which the imprint of the overburden (medium above $z_1$) is
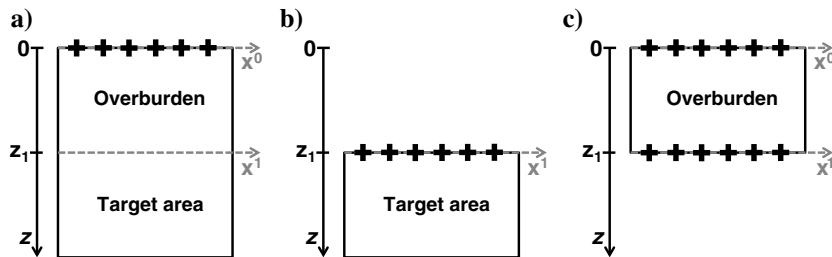


Figure 1. (a) Full medium with free surface, overburden, and target area. (b) Objective medium with the target area below the new datum $z = z_1$ and homogeneous above. (c) Priorly known upper medium with free surface, overburden, and homogeneous below the new datum $z = z_1$. The (virtual) sources and receivers are denoted by the black crosses.

completely removed. This amounts to retrieving the $M \times M$ reflection matrix $\mathbf{R_1^L}$ of the objective medium represented in Figure 1b, which is homogeneous above the new datum $z_1$. The superscript $L$ denotes quantities corresponding to this objective (or lower) medium, and we define $\{R_1^L\}_{ij} = -(4(\Delta x)^2/(\rho(x_i^1)\rho(x_j^1)))$ $\partial_z g^L(x_i^1, x_j^1, \omega)$. The positions of the $M$ virtual sources and receivers at depth $z_1$ (the new datum) are described by the coordinates $x_j^1$ and $x_i^1$, respectively, and $\Delta x$ is the spatial sampling distance of these virtual sensors.

The formal derivation of the redatuming procedure is based on Rayleigh's reciprocity theorem, and it is presented in Appendices A and B. The formulation of the redatuming equations into simple matrix relations explains the peculiar definition of matrix $\mathbf{R_1^L}$ (see equation B-14). In the following, we propose a heuristic, graphics-based illustration of these redatuming equations. The matrices $\mathbf{R}$ and $\mathbf{R_1^L}$ are schematized in Figure 2.

We define $\mathbf{G^+}$ (respectively, $\mathbf{G^-}$) as Green's function matrices in the full medium (Figure 1a) for downward-radiating (respectively, upward-radiating) sources located at depth $z_1$, so that $\{G^+\}_{ij} = (2\Delta x/\rho(x_j^1))g^{p,+}(x_i^0, x_j^1, \omega)$ and $\{G^-\}_{ij} = g^{p,-}(x_i^0, x_j^1, \omega)$ (see equations B-7 and B-10). These matrices are also schematized in Figure 2. If $\mathbf{G^+}$ and $\mathbf{G^-}$ are known, then the reflection matrix $\mathbf{R_1^L}$ can be obtained from the relation

$$\mathbf{G^+} = \mathbf{G^-}\mathbf{R_1^L}, \tag{6}$$

where the matrix product corresponds to a spatial integral along $x^1$. This relation is graphically illustrated in Figure 3a and formally derived in equation B-13. Because the objective medium is homogeneous above depth $z_1$ (Figure 1b), $\mathbf{R_1^L}$ represents the upgoing wavefield response at $z_1$ to a downward-radiating source wavefield at $z_1$. If these upgoing wavefields are convolved with the upward-radiating source Green's function matrix $\mathbf{G^-}$, the resulting wavefield recorded at the free surface is equivalent to the downward-radiating source Green's function matrix $\mathbf{G^+}$.

Note that by virtue of source-receiver reciprocity, knowing $\mathbf{G^+}$ and $\mathbf{G^-}$ is equivalent to measuring upgoing and downgoing wavefields at the new datum, as in a deviated well configuration. Solving for $\mathbf{R_1^L}$ in equation 6 then amounts to a discretized form of interferometry by multidimensional deconvolution (Schuster and Zhou, 2006; Wapenaar and van der Neut, 2010).

Because we do not suppose the physical presence of receivers at depth, we numerically compute $\mathbf{G^+}$ and $\mathbf{G^-}$ using the surface-acquired data set $\mathbf{R}$ and our prior knowledge of the overburden (between $z = 0$ and $z = z_1$). First, we perform numerical simulations in the upper medium depicted in Figure 1c that has a free surface at $z = 0$ and that is homogeneous below $z = z_1$. This gives the reflection and transmission matrices $\mathbf{R^U}$ $(N \times N)$, $\mathbf{R_1^U}$ $(M \times M)$, $\mathbf{T^U}$ $(M \times N)$, and $\mathbf{T_1^U}$ $(N \times M)$, where the superscript U indicates quantities calculated in this upper medium. These matrices are defined as $\{R^U\}_{ij} = g^U(x_i^0, x_j^0, \omega)$, $\{R_1^U\}_{ij} = \partial_z g^U(x_i^1, x_j^1, \omega)$, $\{T^U\}_{ij} = \partial_z g^U(x_i^1, x_j^0, \omega)$, and $\{T_1^U\}_{ij} = g^U(x_i^1, x_j^1, \omega)$ (see equations B-2, B-3, B-7, and B-10). They are graphically represented in Figure 2.

To compute $\mathbf{G^+}$, we then have to build focusing source functions that, when sent from the free surface, collapse into downgoing Dirac impulses at the new datum. Assuming that these focusing functions exist, they can be gathered in the matrix $\mathbf{F^+}$ $(N \times M)$ so that

$$\mathbf{T^U}\mathbf{F^+} = \mathbf{I}, \tag{7}$$

and because the focusing functions are reflected in the upper medium, we define

$$\mathbf{F^-} \equiv \mathbf{R^U}\mathbf{F^+}. \tag{8}$$

The identity matrix $\mathbf{I}$ $(M \times M)$ defines a set of objective Dirac impulses at each position on the new datum. Causality and medium homogeneity below $z_1$ ensure that these are downgoing impulses. The matrix element $\{F^+\}_{ij}$ thus corresponds to the source function to be injected at free-surface position $x_i^0$ to achieve a focus at new datum position $x_j^1$. By definition, $\mathbf{F^-}$ $(N \times M)$ represents the surface response of the focusing functions in the upper medium. The idea of computing the focusing functions $\mathbf{F^+}$ by finding the inverse of the transmission matrix $\mathbf{T^U}$ is at the center of the spatiotemporal inverse-filter technique developed in acoustics (Aubry et al., 2001; Tanter et al., 2001). When the transmission matrix of the overburden is not known, it is possible to compute the focusing functions $\mathbf{F^+}$ and $\mathbf{F^-}$ using an iterative scheme based on a variant of equation 8 and its time-reversed version. This forms the basis of the Marchenko imaging procedure (Rose, 2002; Wapenaar et al., 2013; Broggini et al., 2014) that relies on the reflection response of the medium measured from the surface and a macrovelocity model of the overburden as the only prior knowledge. In contrast, the work presented here relies on a much stronger assumption, i.e., the knowledge of the upper medium parameters, but it allows in turn a more direct way to compute $\mathbf{F^+}$ and $\mathbf{F^-}$ based on the inversion of $\mathbf{T^U}$. Note that the inversion of a transmission operator from a model with sharp contrasts has also been proposed recently to obtain a more accurate initial estimate of $\mathbf{F^+}$ in the Marchenko iterative procedure (Vasconcelos et al., 2015; Vasconcelos and van der Neut, 2016).

By injecting the focusing functions $\mathbf{F^+}$ in the full medium (Figure 1a), we obtain

$$\mathbf{R}\mathbf{F^+} = \mathbf{F^-} + \mathbf{G^+}, \tag{9}$$

where $\mathbf{G^+}$ is the Green's function matrix in the full medium for downward-radiating sources at depth $z_1$. Equation 9 is graphically illustrated in Figure 3b. In the left-side term (respectively, the first
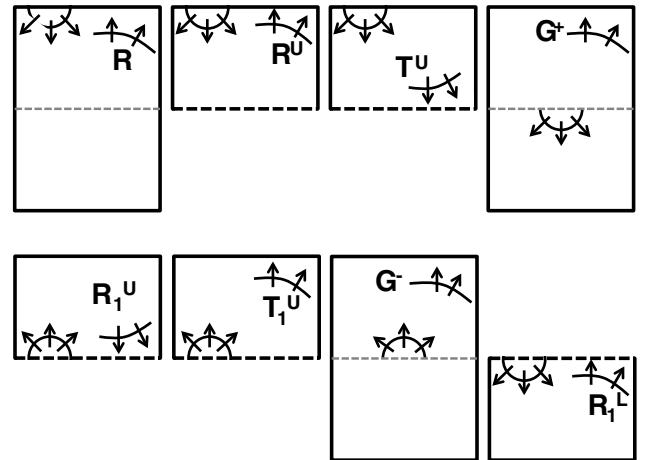


Figure 2. Graphical representation of Green's function matrices used in the redatuming procedure.

term of the right side) of this graphical representation, the emerging (respectively, converging) wavefield at the redatuming level is a consequence of the injection of $\mathbf{F}^+$ in the full (respectively, upper) medium. In the upper medium, we also are reminded that $\mathbf{F}^- \equiv \mathbf{R}^U \mathbf{F}^+$ (equation 8). The Green's functions $\mathbf{G}^+$ emerge as the focusing wavefields create virtual downward-radiating sources at depth $z_1$ in the full medium. By replacing the expressions of the focusing functions $\mathbf{F}^+$ and $\mathbf{F}^-$ (equations 7 and 8) into equation 9, we obtain

$$\mathbf{G}^+ = [\mathbf{R} - \mathbf{R}^U][\mathbf{T}^U]^{-1}. \tag{10}$$

This expression is formally derived in equation B-6.

The matrix $\mathbf{G}^-$ that contains the responses to upward-radiating sources at $z_1$ can be expressed using $\mathbf{G}^+$ as well as the matrices $\mathbf{R}_1^U$ and $\mathbf{T}_1^U$ obtained in the upper medium according to

$$\mathbf{G}^- = \mathbf{T}_1^U + \mathbf{G}^+ \mathbf{R}_1^U. \tag{11}$$

This relation is illustrated in Figure 3c and formally derived in equation B-9. Equation 11 is a decomposition of $\mathbf{G}^-$ into the portion of the wavefield that only travels in the upper medium $\mathbf{T}_1^U$, and the portion of the wavefield that enters the lower medium $\mathbf{G}^+ \mathbf{R}_1^U$. Note that such a decomposition was not necessary in equation 6 because the whole wavefield in $\mathbf{G}^+$ enters the lower medium.

Finally, we replace these expressions of the Green's function matrices $\mathbf{G}^+$ and $\mathbf{G}^-$ into equation 6, to compute the objective virtual data set $\mathbf{R}_1^L$ as
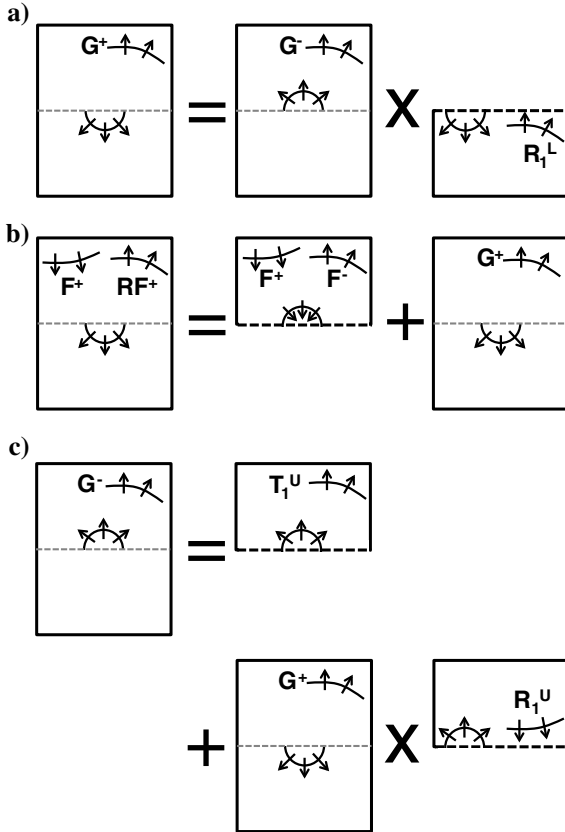


Figure 3. Graphical representation of (a) equation 6, (b) equation 9, and (c) equation 11. To follow the graphics from source to receiver, the matrix products are to be read from right to left.

$$\mathbf{R}_1^L = [\mathbf{G}^-]^{-1} \mathbf{G}^+$$
$$= [\mathbf{T}_1^U + \mathbf{G}^+ \mathbf{R}_1^U]^{-1}[\mathbf{R} - \mathbf{R}^U][\mathbf{T}^U]^{-1}$$
$$= [\mathbf{T}^U[\mathbf{R} - \mathbf{R}^U]^{-1}\mathbf{T}_1^U + \mathbf{R}_1^U]^{-1}. \tag{12}$$

As intended, this expression of the objective reflection matrix $\mathbf{R}_1^L$ (or redatumed data set) is a function only of the initial surface data set $\mathbf{R}$ and of the matrices $\mathbf{R}^U$, $\mathbf{R}_1^U$, $\mathbf{T}^U$, and $\mathbf{T}_1^U$. Note that $\mathbf{R}^U$, $\mathbf{R}_1^U$, $\mathbf{T}^U$, and $\mathbf{T}_1^U$ depend only on the prior knowledge of the overburden.

## NUMERICAL EXAMPLES

### Seismic data set

To illustrate the method, we generate a synthetic seismic data set with 2D acoustic numerical simulations. We use the software developed by Thorbecke and Draganov (2011), based on a finite-difference scheme. The velocity model of the full medium is presented in Figure 4a, and it is 2000 m wide × 2000 m deep. It consists of three homogeneous layers separated by two nonhorizontal boundaries, of which velocities are 1600, 2200, and 2800 m/s, and of which densities are 1000, 2000, and 3000 kg/m³. The new datum is
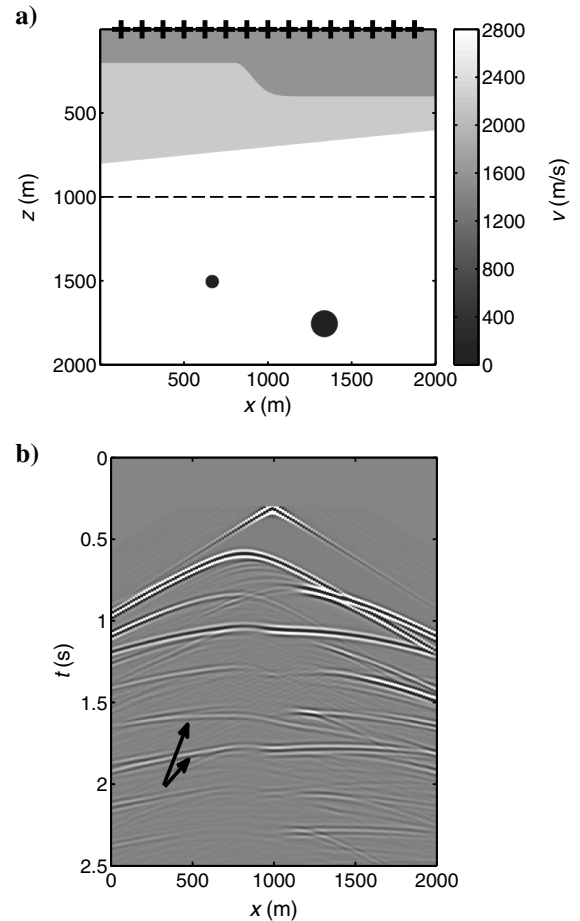


Figure 4. (a) Full seismic medium including the free surface, the overburden, and the two targets. A subpart of the sources and receivers are denoted by the black crosses. (b) Common-source gather for a source at $x = 992$ m. The two black arrows indicate the primary scattering events from the targets.

located below the first two layers at depth $z = 1000$ m. Two circular inclusions with vanishing velocity and diameters 80 and 160 m are placed in the homogeneous third layer, below the new datum, and they represent the targets to be detected. We have free-surface boundary conditions at the upper boundary and absorbing conditions at the other boundaries.

The initial reflection data set **R** is generated using $N = 126$ sources and receivers located a quarter wavelength below the free surface, corresponding to a sensor spacing of 16 m. The monopole (explosive) sources are modeled with a Ricker wavelet with a center frequency of 25 Hz. The spatial step of the grid is 4 m, and the temporal step is 0.8 ms. An example of a common-source gather shows primary and multiple scattering events from the overburden and the two targets (Figure 4b). The primary scattering events from the targets, partially screened by overburden multiples, arrive at 1.6 and 1.9 s at $x = 0$ m (see the black arrows in Figure 4b).

The redatuming procedure starts with simulations in the upper medium that corresponds to our prior knowledge of the overburden (Figure 5a). We place $N = 126$ sources and receivers a quarter wavelength below the free surface and another $M = 126$ sources and receivers at the new datum. This allows us to calculate the reflection and transmission matrices $\mathbf{R}^U$, $\mathbf{R}_1^U$, $\mathbf{T}^U$, and $\mathbf{T}_1^U$. We compute the focusing functions $\mathbf{F}^+ = [\mathbf{T}^U]^{-1}$ (see equation 7) using a truncated singular-value decomposition (SVD) for the inversion of $\mathbf{T}^U$. We then construct the downward-radiating and upward-radiating Green's function matrices $\mathbf{G}^+$ and $\mathbf{G}^-$ following equations 10 and 11. Finally, we compute the objective redatumed data set $\mathbf{R}_1^L$ following the first line of equation 12. The inverse of $\mathbf{G}^-$ is obtained using another truncated SVD.

An example of a common-source gather from the redatumed data set is shown in Figure 6a (the source at $x = 992$ m). The two dominant events correspond to primary scattering on the two targets (see the black arrows), and the two following events correspond to target multiples (white arrows). As intended, the redatumed data set corresponds to a virtual acquisition made at depth $z = 1000$ m, for which the imprint of the overburden is completely removed. For comparison, a synthetic version of the objective data set is shown in Figure 6b. This synthetic data set is obtained from a numerical simulation performed in the objective medium shown in Figure 5b. We also present a comparison of three individual traces from the redatumed and synthetic data sets corresponding to three different receiver positions: $x = 656$ m, $x = 992$ m, and $x = 1328$ m (Figure 7).

The two primaries and first two multiples are observed in the redatumed and the synthetic data sets. The difference in shape and amplitude of the events with increasing offset is caused by the limited aperture of the free-surface array. For instance, an amplitude reduction is observed for the primary scattering event arriving at approximately $t = 0.9$ s at $x = 656$ m in Figure 7 (the black arrow). Some weak acausal events are present in the redatumed data set (in the shaded areas). These events are again related to the finite aperture of the free-surface array, and they are caused by the diffraction of the focusing function emitted at the edges of the array. This effect
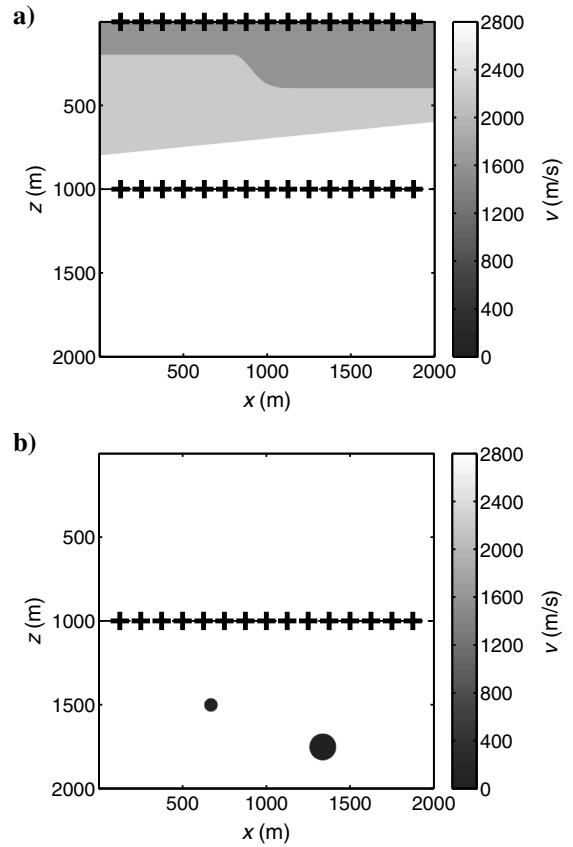


Figure 5. (a) Upper medium with free surface, overburden, and homogeneous conditions below the new datum $z = 1000$ m. (b) Objective medium with two targets below the new datum $z = 1000$ m and homogeneous conditions above. A subpart of the (virtual) sources and receivers are denoted by the black crosses.
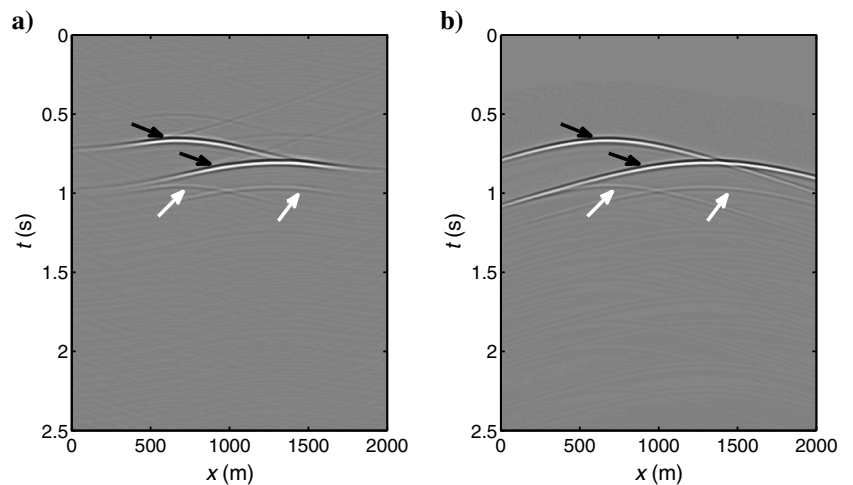


Figure 6. Common-source gather from: (a) the redatumed seismic data set $\mathbf{R}_1^L$ and (b) a synthetic numerical simulation in the objective medium. The (virtual) source is located at position $x = 992$ m along the new datum. The two black arrows indicate the primary scattering events from the targets. The two white arrows indicate the first two multiple-scattering events from the targets.

could possibly be attenuated using spatial tapering techniques during the inversion of the focusing function. The attenuation of these artifacts, also expected to occur in standard redatuming techniques, is beyond the scope of this study.

In this example, we assumed a perfect prior knowledge of the overburden to estimate its reflection and transmission matrices $\mathbf{R}^U$, $\mathbf{R}_1^U$, $\mathbf{T}^U$, and $\mathbf{T}_1^U$. In seismic studies, having detailed knowledge of the overburden is rare; often, only a smoothed velocity model of the overburden might be available as prior information. To test the redatuming procedure in such a case, we repeat the previous example, this time using a smoothed version of the upper medium. We apply a running average of 80 m along the depth dimension of the slowness model of the overburden. The smoothing length corresponds to one central wavelength in the first layer of the overburden. The obtained smoothed upper medium is presented in Figure 8a. We run numerical simulations in this smooth upper medium to obtain the reflection and transmission matrices $\mathbf{R}^U$, $\mathbf{R}_1^U$, $\mathbf{T}^U$, and $\mathbf{T}_1^U$. The rest of the procedure remains the same, and a common-source gather from the redatumed data set is shown in Figure 8b (with the source at $x = 992$ m).

Although the two primary scattering events on the targets are still visible (see the black arrows), these redatumed data are dominated by acausal and unphysical events. The use of a smooth upper medium does not allow us to model internal multiples in the overburden. These multiples are thus not correctly handled in the focusing functions, and they create unphysical events in the virtual-source Green's functions $\mathbf{G}^+$ and $\mathbf{G}^-$. These unphysical events then interfere with the multidimensional deconvolution procedure and appear in the redatumed data set.

## Acoustic data set

We generate another synthetic data set with 2D acoustic numerical simulations. This time, we use reflective side boundaries to simulate a typical configuration encountered in acoustic nondestructive testing of finite-size material samples. We use a custom-made acoustic finite-difference scheme with constant density. We use the same velocity model, downsized to 1 m wide × 1 m deep (Figure 9a). The new datum is now located at depth $z = 50$ cm, and the two circular targets are of diameter 4 and 8 cm. We apply free-surface boundary conditions at the top ($z = 0$), left ($x = 0$), and right ($x = 100$ cm) boundaries and an absorbing boundary condition at the bottom boundary ($z = 100$ cm).

The initial reflection data set $\mathbf{R}$ is generated using $N = 125$ sources and receivers located one grid point (0.5 mm) below the free surface, corresponding to sensor spacing of 0.8 cm. The monopole (explosive) sources are modeled with a Ricker wavelet with a center frequency of 50 kHz. The spatial step of the grid is 0.5 mm, and the temporal step is 0.11 μs. An example of a common-source gather shows primary and multiple scattering events from the overburden, the two targets, and the side boundaries (Figure 9b). The primary scattering events from the targets, partially screened by overburden multiples and side reflections, arrive at 1 and 1.2 ms at $x = 0$ cm (see the black arrows in Figure 9b).

We follow the first procedure detailed in the previous section (no smoothing applied) to compute the objective redatumed data set $\mathbf{R}_1^L$. An example of a common-source gather from the redatumed data set is shown in Figure 10a (source at $x = 50$ cm). The two dominant events correspond to primary scattering on the two targets (black
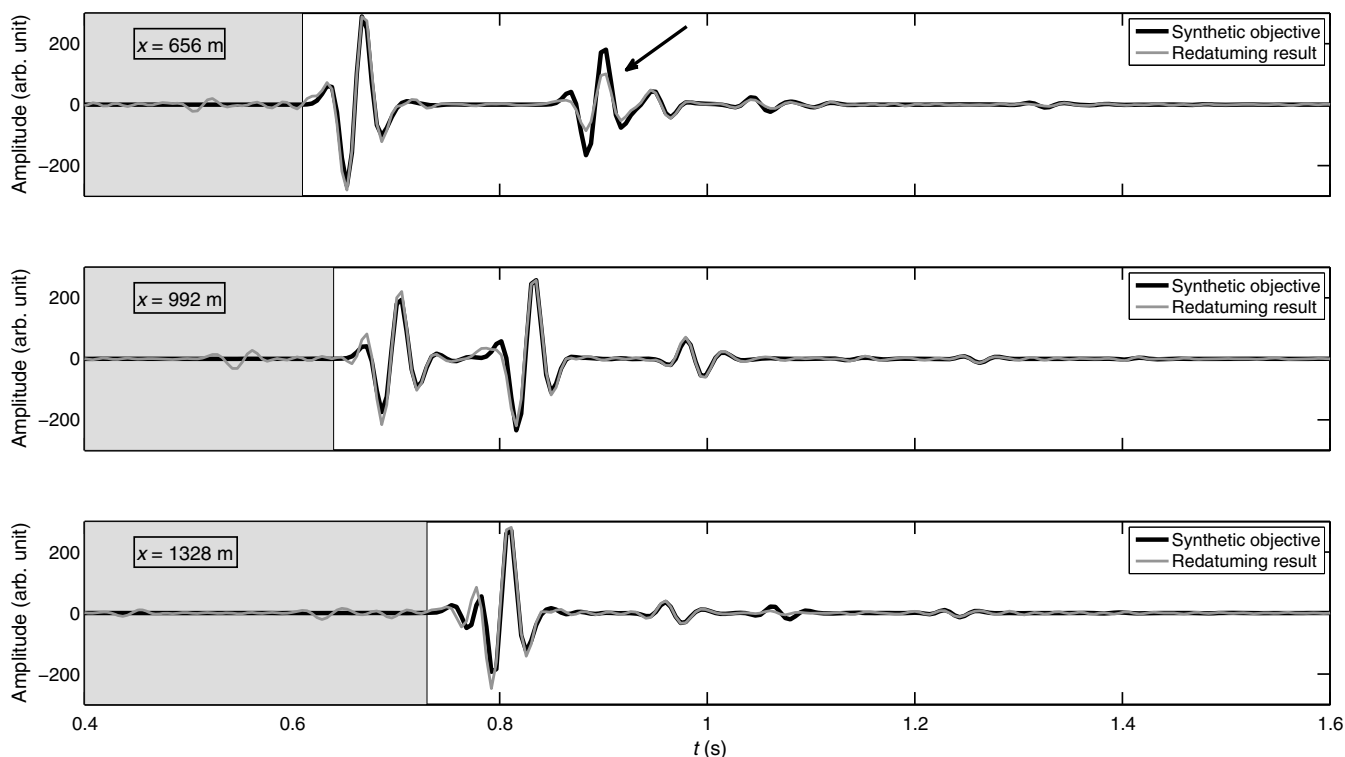


Figure 7. Comparison of redatumed and synthetic seismic traces at three different receiver positions: $x = 656$ m, $x = 992$ m, and $x = 1328$ m. The (virtual) source is located at position $x = 992$ m along the new datum. The shaded area represents the acausal time period before the first scattering event.

arrows), and the next two events correspond to the first two multiple-scattering interactions of the targets (white arrows). The following events correspond to a combination of target and side-boundary multiples. As intended, the redatumed data set corresponds to a virtual acquisition made at depth $z = 50$ cm, and for which the imprint of the overburden is completely removed. For comparison, a synthetic version of the objective data set is shown in Figure 10b. We also present a comparison of three individual traces from the redatumed and synthetic data sets corresponding to three different receiver positions: $x = 33$ cm, $x = 50$ cm, and $x = 66$ cm (Figure 11).

A good agreement is observed between the redatumed and the synthetic data set until approximately $t = 0.7$ ms. In contrast with the absorbing-side-boundaries case (Figure 6a), the differences in shape and amplitude of the early events with increasing offset are much less pronounced (Figure 10a). The acausal events due to diffraction of the focusing function at the edges of the free-surface array are also less noticeable (shaded areas in Figure 11). The presence of the reflective side boundaries increases the effective aperture of the free-surface array and thus improves the

reconstruction of the redatumed data set. This effective aperture still remains limited, as indicated by the substantial differences between traces at late times (after $t = 0.7$ s in Figure 11). To obtain a perfect match between the redatumed traces and the synthetic data, a perfect angular coverage of illumination would be required at the redatuming level. This could only be achieved by embedding sources along the side boundaries of the sample.

## DISCUSSION

The redatuming procedure that we propose requires a detailed knowledge of the overburden, with sharp interfaces and accurate reflection and transmission coefficients. This is the most significant challenge toward possible seismic applications of this method. The use of smooth overburden models does not allow to account for multiples in the focusing functions, and it leads to strong artifacts in the redatuming result (Figure 8b). We foresee that only simple overburden cases could be known with enough precision for correct handling of multiples in the focusing functions. Such precise overburden models could be obtained through a preliminary application
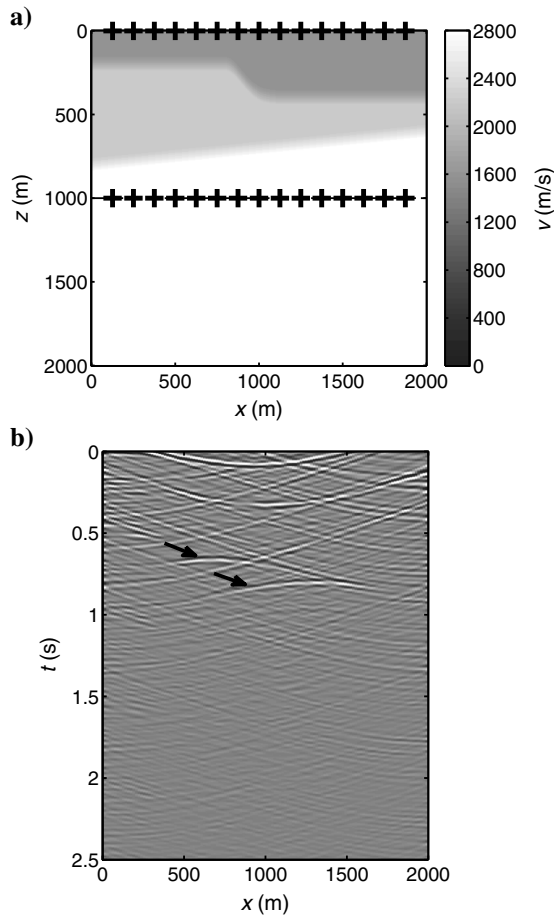


Figure 8. (a) Upper medium with free surface, smoothed overburden, and homogeneous conditions below the new datum $z = 1000$ m. (b) Common-source gather from the redatumed seismic data set obtained with the smoothed upper medium. The virtual source is located at position $x = 992$ m along the new datum. The two black arrows indicate the primary scattering events from the targets.
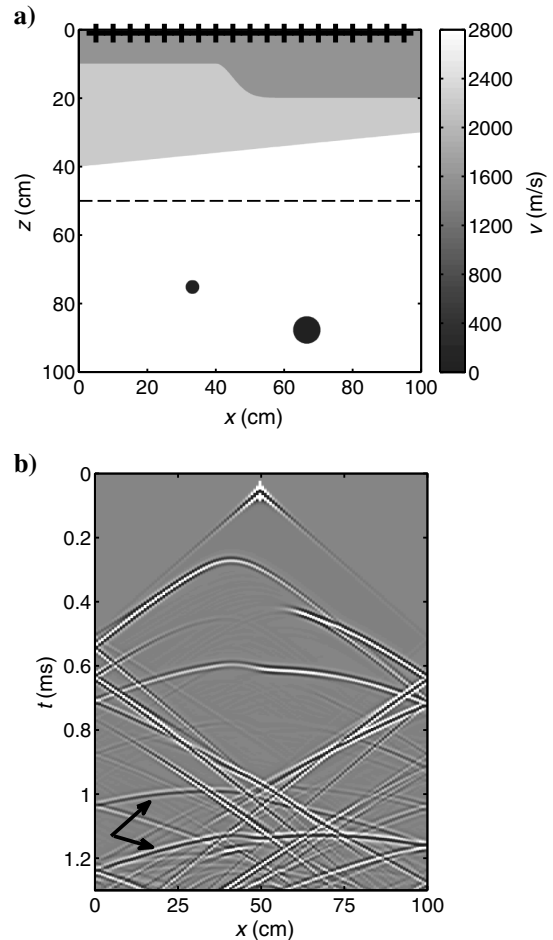
Figure 9. (a) Full acoustic medium including the free surface at the top and side boundaries, the overburden, and the two targets. A subpart of the sources and receivers is denoted by the black crosses. (b) Common-source gather with source at position $x = 50$ cm. The two black arrows indicate the primary scattering events from the targets.

of reverse time migration or full-waveform-inversion techniques. A first step toward applications to real data would be to try to re-datum marine data below an ocean bottom with irregular topography. In that case, only the water column and a single solid layer would have to be modeled.

For acoustic nondestructive-testing application purposes, this constraint can be less significant. In some instances, the transmission and reflection matrices of the overburden can be physically measured (Aubry et al., 2001). This is the case when the medium to image is covered by insulating layers and when those insulating layers can be submitted to acoustic measurements before installation.

A redatuming procedure similar to the one that we propose was already introduced by Mulder (2005) and called rigorous redatuming. It also requires detailed knowledge of the overburden and aims to fully remove its imprint in the redatumed data set. To derive his method, Mulder (2005) uses equivalent source terms in the wave equation to impose specific wavefields at the redatuming level. The practical implementation of his method involves solving a sequence of three inverse problems. In contrast, our approach is formally derived using a combination of one-way and two-way reciprocity theorems. We also introduced a heuristic graphics-based derivation to illustrate the connections with the inverse filter method (Tanter et al., 2001) and the Marchenko imaging method (Wapenaar et al., 2013). The practical implementation of our method involves solving two inverse problems: one to obtain the focusing function $\mathbf{F}^+$ and one to implement the multidimensional deconvolution procedure. Note that our final redatumed data set corresponds to the vertical derivative of the pressure and not to the pressure itself (equation B-14). We chose this convention because it required the least amount of processing steps. Had we de-
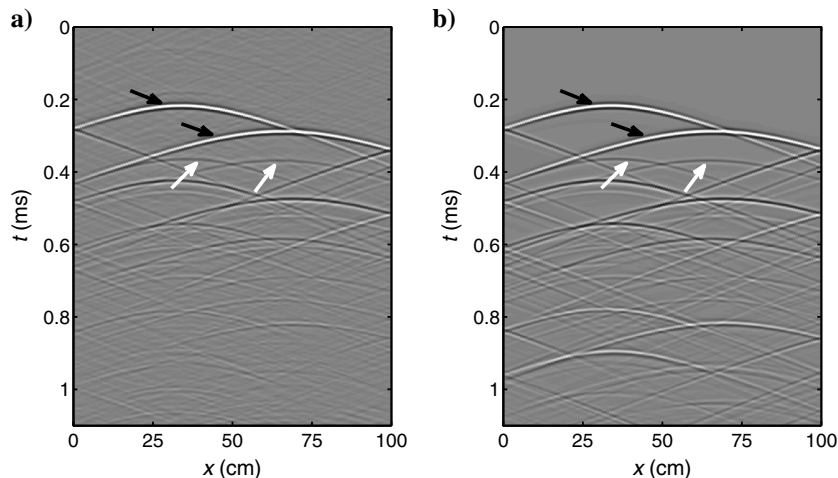


Figure 10. Common-source gather from (a) the redatumed acoustic data set $\mathbf{R}_1^{\mathbf{L}}$ and (b) a synthetic numerical simulation in the objective medium. The (virtual) source is located at position $x = 50$ cm along the new datum. The two black arrows indicate the primary scattering events from the targets. The two white arrows indicate the first two multiple-scattering events from the targets.
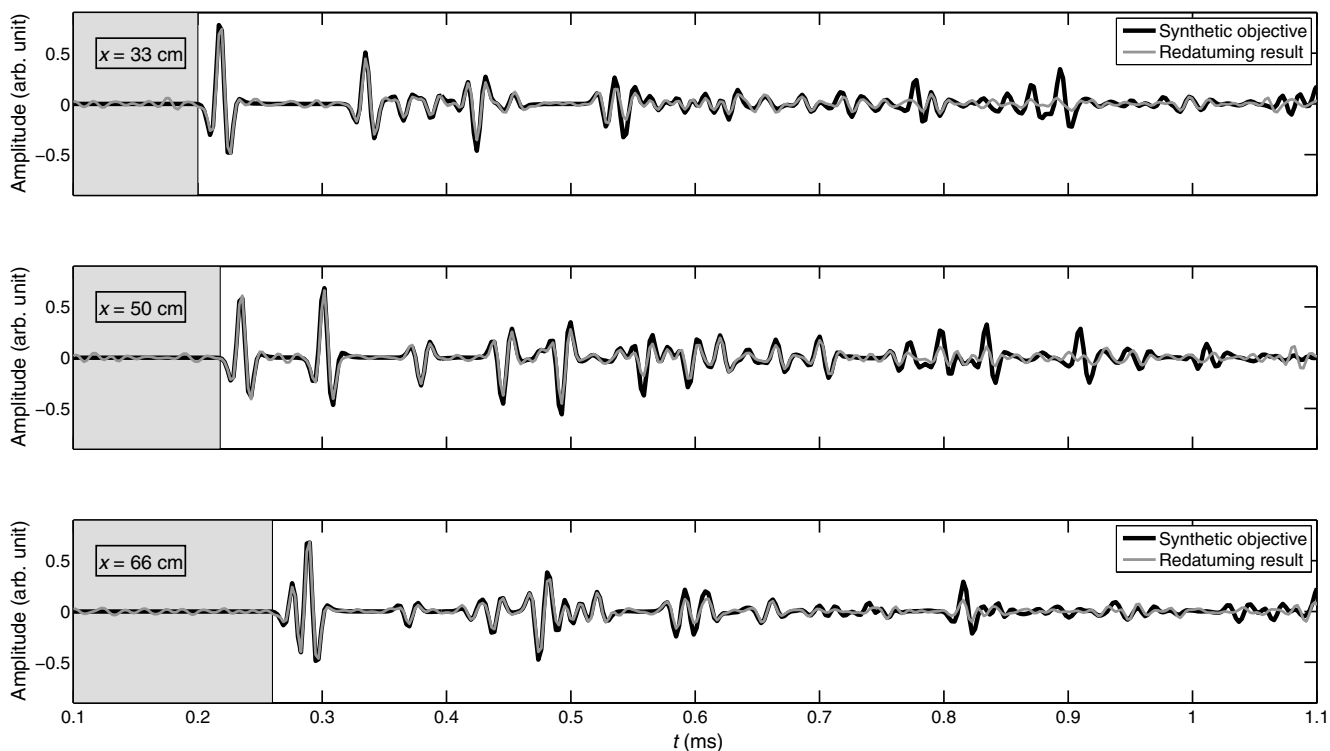


Figure 11. Comparison of redatumed and synthetic acoustic traces at three different receiver positions: $x = 33$ cm, $x = 50$ cm and $x = 66$ cm. The (virtual) source is located at position $x = 50$ cm along the new datum. The shaded area represents the acausal time period before the first scattering event.

cided to retrieve the pressure wavefield (as is done by Mulder, 2005), a third inversion step would have been required.

Our method and the Marchenko imaging procedure involve creating upward-radiating and downward-radiating virtual sources at the new datum. Once the surface responses to these virtual sources are retrieved, the very same step of multidimensional deconvolution is required to estimate the reflection matrix of the objective medium ($\mathbf{R}_1^{\mathbf{L}}$) for the two methods. To create the virtual sources at the new datum, the Marchenko procedure aims to build focusing functions through an iterative process. The strength of the method is that it only requires a smooth velocity model of the overburden as prior knowledge. This makes the method well-suited for most seismic applications. However, the original Marchenko method also presents restrictions because it cannot handle attenuative media or irregular free-surface topography. The iterative construction of the focusing functions is based on the correlation-type one-way reciprocity theorem that is only valid for lossless media (Wapenaar and Grimbergen, 1996). Handling dissipative media within the Marchenko framework is part of ongoing research (Zhang et al., 2016). A flat free surface can be incorporated in the original Marchenko procedure (Singh et al., 2015) but not a free surface with irregular topography. Note that a new formulation of the Marchenko scheme was recently proposed to handle a free surface with irregular topography (Ravasi, 2017; Slob and Wapenaar, 2017), provided that an up/down decomposition of the wavefield can be performed at the receiver level.

In comparison, the redatuming method that we propose requires a much more detailed prior knowledge of the overburden. In turn, a single inversion step allows us to compute the focusing functions and to account for factors such as attenuation, dispersion, irregular surface topography, and irregular spatial sampling. Attenuation is correctly handled because we only rely on convolution-type reciprocity theorems (Wapenaar and Grimbergen, 1996). Irregular surface topography and irregular spatial sampling are made possible by the use of a combined two-way/one-way reciprocity theorem (equation A-5). Note that the irregular spatial sampling has to be considered within some limits to ensure adequate illumination of the medium. Minato et al. (2013) discuss how to find optimum illumination parameters based on an SVD approach to solve the inverse problem of multidimensional deconvolution. The aperture of the free surface array also influences the radiation pattern of the virtual sources at the redatuming level. In practice, the depth of the new datum should be kept much smaller than the aperture of the free surface array to ensure adequate illumination of the target area.

The derivation of the one-way reciprocity theorems requires that no reflector should cross the redatatuming level (Wapenaar and Berkhout, 1989, Appendix B). In practice, we do not expect this situation to generate significant artifacts. Indeed, the same assumption applies to the Marchenko procedure, and several studies have shown successful reconstruction of virtual sources along redatuming levels crossed by reflectors (Broggini et al., 2014; Singh and Snieder, 2017). Similar to the original Marchenko procedure, our redatuming method requires the knowledge of the source wavelet. In all acquired and simulated data, a preliminary deconvolution of the source wavelet is implicitly assumed in our derivation that only uses Green's functions.

The extension of the method to 3D acoustic data should be straightforward; however, the application to elastic data should be carefully tested. Based on recent progresses in elastic Marchenko imaging (da Costa Filho et al., 2014; Wapenaar, 2014), we believe that elastic redatuming could also be achieved. The limitation in the elastic case would probably come from the ability to have a detailed knowledge of many more model parameters.

## CONCLUSION

We introduced a model-based redatuming technique that correctly handles surface multiples and internal multiples in the overburden. The technique relies on the assumption that a detailed knowledge of the model parameters is available above the new datum.

We provided a formal derivation of the redatuming equations based on convolution-type reciprocity theorems. We also presented an intuitive graphics-based derivation supported by a matrix formalism. This heuristic derivation allowed us to connect our redatuming method with the previously developed inverse-filter technique and Marchenko imaging procedure. The practical implementation of the redatuming procedure can be summarized as follows:

1)  Use numerical simulations to estimate reflection and transmission matrices of the overburden.
2)  Through an inversion step, retrieve the focusing functions that give rise to downward-radiating virtual sources at the new datum.
3)  Use the initial data set collected at the free-surface and the simulated overburden matrices to compute the surface responses to downward-radiating and upward-radiating virtual sources at the new datum.
4)  Use the responses to these virtual sources to evaluate the redatumed data set through multidimensional deconvolution.

The redatumed data set corresponds to a virtual reflection response acquired at the new datum and for which the imprint of the overburden is completely removed.

We demonstrated the procedure on two synthetic data sets generated in 2D acoustic media. The first medium had absorbing side boundaries to simulate a seismic data set, whereas the other medium had free-surface side boundaries to simulate an acoustic nondestructive-testing data set. In both cases, the redatuming procedure allowed us to retrieve primary and multiple scattering events from targets located below the overburden. The absence of surface multiples and internal multiples showed that the imprint of the overburden was fully removed. The redatumed seismic data set suffered from finite-aperture effects of the free-surface array, as can be expected from any other standard redatuming procedure. The redatumed acoustic data set suffered from these limitations much less because the reflective side boundaries artificially increased the effective aperture of the free-surface array. We also tested the technique in the case for which only a smooth velocity model of the overburden is known as prior information. The method did not function in that instance because such a smooth prior model did not allow us to model internal multiples for the construction of the focusing functions.

This technique requires a more detailed prior knowledge than the Marchenko imaging procedure to compute the focusing functions. However, it can provide a more direct way to perform the redatuming in cases for which such detailed knowledge of the overburden is available. Indeed, the interest of the technique lies in the fact that the inversion of the transmission matrix automatically generates a focus free of multiples and compensates for effects such as attenuation, irregular topography, and irregular spatial sampling.

## APPENDIX A

## RECIPROCITY THEOREMS

Consider two independent wave states $A$ and $B$, defined by medium parameters $(\rho_A, \kappa_A)$ and $(\rho_B, \kappa_B)$ and source terms $f_A$ and $f_B$. If inside a volume $V$ enclosed by a surface $S$, the medium parameters are the same for state $A$ and state $B$, a special case of Rayleigh's reciprocity theorem (Wapenaar and Berkhout, 1989, chapter 5.2) gives

$$\oint_S \frac{1}{\rho}[p_A \nabla p_B - p_B \nabla p_A].d\mathbf{S} = \int_V \frac{1}{\rho}[p_A f_B - p_B f_A]dV.$$
(A-1)

This relation is valid for arbitrary and independent source terms $f_A$ and $f_B$. The medium parameters outside the integration volume $V$ can also be different for states $A$ and $B$. By choosing $f_B = \rho(\mathbf{r})\delta(\mathbf{r} - \mathbf{r_0})$, with $\mathbf{r_0}$ inside $V$ and $f_A = 0$, we obtain the special case known as the representation theorem:

$$p(\mathbf{r_0}) = \oint_S \frac{1}{\rho}[p(\mathbf{r})\nabla g(\mathbf{r}, \mathbf{r_0}) - g(\mathbf{r}, \mathbf{r_0})\nabla p(\mathbf{r})] \cdot d\mathbf{S}. \quad (A-2)$$

### Case with a free surface

Consider a volume $V$ enclosed by a surface $S$ composed of a free surface and a virtual horizontal boundary $S_1$ at an arbitrary depth, as represented in Figure A-1a. The coordinate $x^1$ denotes the horizontal position along the boundary $S_1$ and $z$ is the depth coordinate.
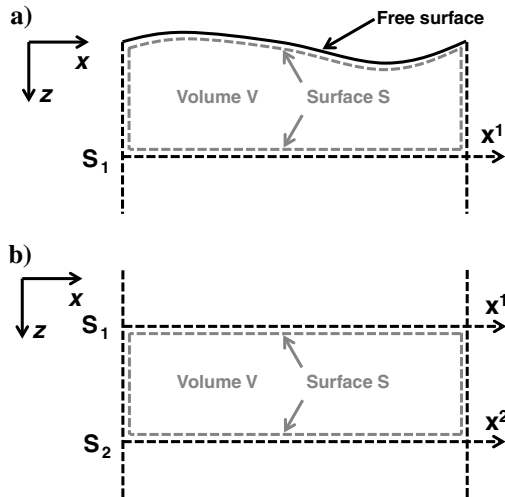


Figure A-1. Schematic representation of the integration volumes for the derivation of the reciprocity theorems (a) with a free surface and (b) without a free surface.

Because the pressure vanishes at the free surface and because the boundary $S_1$ is orthogonal to the $z$-axis, the reciprocity theorem (equation A-1) simplifies to

$$\int_{S_1} \frac{1}{\rho(x^1)}[p_A(x^1)\partial_z p_B(x^1) - p_B(x^1)\partial_z p_A(x^1)]dx^1$$

$$= \int_V \frac{1}{\rho}[p_A f_B - p_B f_A]dV.$$
(A-3)

This also supposes that the depth of $S_1$ is much smaller than the medium width, so that the side contributions to the surface integral can be neglected. By decomposing $p_A$ and $p_B$ as upgoing and downgoing wavefields at $S_1$, the left side of equation A-3 can be expanded into the four following terms:

$$\int_{S_1} \frac{1}{\rho(x^1)}[p_A^+ \partial_z p_B^- + p_A^- \partial_z p_B^+]dx^1$$

$$+ \left[ -\int_{S_1} \frac{1}{\rho(x^1)}[p_B^+ \partial_z p_A^- + p_B^- \partial_z p_A^+]dx^1 \right]$$

$$+ \int_{S_1} \frac{1}{\rho(x^1)}[p_A^+ \partial_z p_B^+ + p_A^- \partial_z p_B^-]dx^1$$

$$+ \left[ -\int_{S_1} \frac{1}{\rho(x^1)}[p_B^+ \partial_z p_A^+ + p_B^- \partial_z p_A^-]dx^1 \right].$$
(A-4)

Assuming that there are no reflectors crossing the boundary $S_1$, i.e., $\partial_z \rho(x^1) = 0$ and $\partial_z \kappa(x^1) = 0$, the upgoing and downgoing wavefields are locally decoupled. Using the pressure-normalized one-way wave equation at $S_1$, it can be shown that the first and second terms of expression A-4 are equal to each other, and that the third and fourth terms cancel each other out (Wapenaar and Berkhout, 1989, Appendix B). The reciprocity theorem can thus be written as

$$\int_{S_1} \frac{2}{\rho(x^1)}[p_A^+(x^1)\partial_z p_B^-(x^1) + p_A^-(x^1)\partial_z p_B^+(x^1)]dx^1$$

$$= \int_V \frac{1}{\rho}[p_A f_B - p_B f_A]dV.$$
(A-5)

This special form of the reciprocity theorem is used in the next section to derive equations B-6 and B-9 of the redatuming technique. The boundary $S_1$ corresponds to the redatuming level, which should not be crossed by a reflector for the method to be strictly valid.

We also use equation A-5 to derive an identity that is used in the following. For wave state $A$, let us consider the case of an impulsive source $f_A = \rho\delta(x^1 - x_i^1)$ at a distance $\varepsilon \to 0$ above $x_i^1$. For wave state $B$, an impulsive source $f_B = \rho\delta(x^1 - x_j^1)$ is located at a distance $\varepsilon \to 0$ below $x_j^1$. Assuming that the medium is homogeneous outside the volume $V$, equation A-5 simplifies to

$$\int_{S_1} \frac{2}{\rho(x^1)} p_A(x^1)\partial_z p_B^-(x^1)dx^1 = -p_B(x_i^1), \quad (A-6)$$

where we note that $p_A^-(x^1) = 0$ and thus $p_A(x^1) = p_A^+(x^1)$. We also used the fact that $f_B = 0$ in the integration volume $V$. As epsilon goes to zero, the wave states $A$ and $B$ become symmetrically equivalent and we have $p_A(x_j^1) = p_B(x_i^1)$. We then deduce from equation A-6 the identity

$$\partial_z p_B^-(x^1) = -\frac{\rho(x^1)}{2}\delta(x^1 - x_j^1). \qquad \text{(A-7)}$$

This expression describes the vertical derivative of the upgoing pressure field just above an impulsive source. A similar expression is used in the derivation of the pressure-normalized Marchenko equations by Wapenaar et al. (2014, equation A-8).

## Case without a free surface

Consider now a volume $V$ enclosed by a surface $S$ composed of two virtual horizontal boundaries $S_1$ and $S_2$, as represented in Figure A-1b. The coordinate $x^1$ (respectively $x^2$) denotes the horizontal position along the boundary $S_1$ (respectively $S_2$), and $z$ is the depth coordinate. Because the surface $S$ enclosing the volume $V$ does not include a free surface, the surface integral needs to be expressed at $S_1$ and $S_2$. We further assume that there are no sources in the volume $V$, so that the reciprocity theorem (equation A-1) simplifies to

$$\int_{S_1} \frac{1}{\rho(x^1)}[p_A(x^1)\partial_z p_B(x^1) - p_B(x^1)\partial_z p_A(x^1)]\mathrm{d}x^1$$
$$= \int_{S_2} \frac{1}{\rho(x^2)}[p_A(x^2)\partial_z p_B(x^2) - p_B(x^2)\partial_z p_A(x^2)]\mathrm{d}x^2.$$
$$\text{(A-8)}$$

Similar to the previous case, we use the upgoing and downgoing wavefield decomposition at boundaries $S_1$ and $S_2$. Assuming that there are no reflectors crossing $S_1$ and $S_2$, we obtain the one-way reciprocity theorem of the convolution type (Wapenaar et al., 2014, Appendix):

$$\int_{S_1} \frac{1}{\rho(x^1)}[p_A^+(x^1)\partial_z p_B^-(x^1) + p_A^-(x^1)\partial_z p_B^+(x^1)]\mathrm{d}x^1$$
$$= \int_{S_2} \frac{1}{\rho(x^2)}[p_A^+(x^2)\partial_z p_B^-(x^2) + p_A^-(x^2)\partial_z p_B^+(x^2)]\mathrm{d}x^2.$$
$$\text{(A-9)}$$

This relation is used in the next section to derive equation B-13 of the redatuming technique. The boundary $S_1$ corresponds to the redatuming level, and the boundary $S_2$ is virtually located below the deepest reflector of the full medium.

## APPENDIX B

## DERIVATION OF THE REDATUMING EQUATIONS

### Definition of the different wave states

We define four different wave states that are used with the reciprocity theorems to derive the redatuming equations (Figure B-1). The full medium is represented in state A, with an irregular free surface. The original reflection data acquisition is made along the boundary $S_0$ at an arbitrary depth below the free surface. The boundary $S_0$ can be curvilinear, and the acquisition spatial interval can be irregular. The positions of sources and receivers along the boundary $S_0$

are denoted by the coordinate $x^0$. The new datum boundary $S_1$ is located below the overburden and is set to be horizontal. The positions along the new datum are denoted by the coordinate $x^1$, and the spatial interval $\Delta x$ is chosen to be constant. The target area lies below the new datum $S_1$.

For an impulsive pressure source located at position $x_i^0$, the reflection response $R(x^0, x_i^0) \equiv g(x^0, x_i^0)$ is the pressure recorded along $x^0$. We also define the downgoing (respectively, upgoing) pressure wavefield at $x^1$ $g^{+,p}(x^1, x_i^0)$ (respectively, $g^{-,p}(x^1, x_i^0)$). By reciprocity (equation 5), these can be seen as the pressure response at $x_i^0$ for an upward-radiating (respectively, downward-radiating) impulsive source at $x^1$ $g^{p,-}(x_i^0, x^1)$ (respectively, $g^{p,+}(x_i^0, x^1)$). These last two Green's functions are the ones that we aim to determine to achieve the redatuming. In summary, we have

$$f_A = \rho\delta(x^0 - x_i^0),$$
$$p_A(x^0) = R(x^0, x_i^0) \equiv g(x^0, x_i^0),$$
$$p_A^+(x^1) = g^{p,-}(x_i^0, x^1) \equiv g^{+,p}(x^1, x_i^0),$$
$$p_A^-(x^1) = g^{p,+}(x_i^0, x^1) \equiv g^{-,p}(x^1, x_i^0). \qquad \text{(B-1)}$$

Wave states B and C take place in the upper medium that represents the overburden and that extends from the free surface to the new datum $S_1$. The medium below the new datum is homogeneous. We run two different simulation sets in this upper medium. For wave state B, an impulsive pressure source is placed at $x_j^0$ and the reflection response $R^U(x^0, x_j^0) \equiv g^U(x^0, x_j^0)$ from $S_0$ to $S_0$ is recorded along $x^0$. The transmission response $T^U(x^1, x_j^0) \equiv g^{U|+,p}(x^1, x_j^0)$ from $S_0$ to $S_1$ is also recorded. We have

$$f_B = \rho\delta(x^0 - x_j^0),$$
$$p_B(x^0) = R^U(x^0, x_j^0) \equiv g^U(x^0, x_j^0),$$
$$\partial_z p_B^+(x^1) = \partial_z T^U(x^1, x_j^0) \equiv \partial_z g^{U|+,p}(x^1, x_j^0),$$
$$\partial_z p_B^-(x^1) = \partial_z g^{U|-,p}(x^1, x_j^0) = 0, \qquad \text{(B-2)}$$
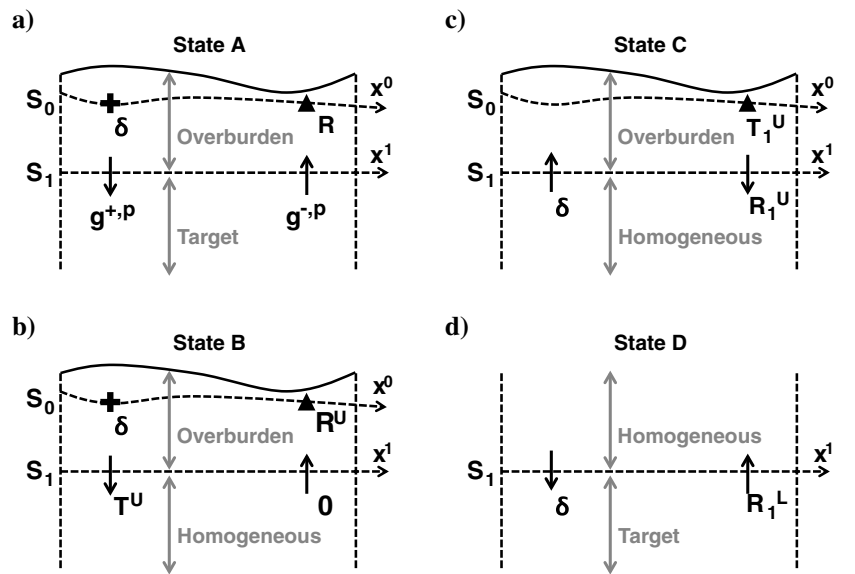


Figure B-1. Illustration of wave states $A$, $B$, $C$, and $D$ used in the reciprocity theorems for the derivation of the redatuming equations.

where the superscript $U$ denotes quantities computed in the upper medium. The upper medium being homogeneous below the new datum, no energy can propagate upward at the redatuming level.

For wave state C, an impulsive pressure source is placed at $x_k^1$, and the reflection response from $S_1$ to $S_1$ in the upper medium $R_1^U(x^1, x_k^1) \equiv g^U(x^1, x_k^1)$ is recorded along $x^1$. The transmission response $T_1^U(x^0, x_k^1) \equiv g^U(x^0, x_k^1)$ from $S_1$ to $S_0$ is also recorded. We have

$$
\begin{aligned}
f_C &= \rho\delta(x^1 - x_k^1), \\
p_C(x^0) &= T_1^U(x^0, x_k^1) \equiv g^U(x^0, x_k^1), \\
\partial_z p_C^+(x^1) &= \partial_z R_1^U(x^1, x_k^1) \equiv \partial_z g^U(x^1, x_k^1), \\
\partial_z p_C^-(x^1) &= -\rho\delta(x^1 - x_k^1)/2,
\end{aligned}
\tag{B-3}
$$

where the source is located at a distance $\varepsilon \to 0$ below $S_1$. The expression of $\partial_z p_C^-$ was derived in the previous section (equation A-7). We note that to comply with the strictly downgoing character of $p_C^+$, the practical implementation of this step should include the removal from $R_1^U(x^1, x_k^1)$ of the direct wave that propagates quasi-horizontally.

Wave state D takes place in the objective medium that represents the target area below the new datum $S_1$. The medium above the new datum is homogeneous. The redatumed or objective data set corresponds to an acquisition made along $S_1$. For an impulsive pressure source at $x_l^1$, the pressure wavefield measured at $x^1$ forms the reflection response $R_1^L(x^1, x_l^1) \equiv g^L(x^1, x_l^1)$. We have

$$
\begin{aligned}
f_D &= \rho\delta(x^1 - x_l^1), \\
\partial_z p_D^+(x^1) &= \rho\delta(x^1 - x_l^1)/2, \\
\partial_z p_D^-(x^1) &= \partial_z R_1^L(x^1, x_l^1) \equiv \partial_z g^L(x^1, x_l^1),
\end{aligned}
\tag{B-4}
$$

where the superscript $L$ denotes quantities related to the objective (or lower) medium. The source is located at a distance $\varepsilon \to 0$ above $S_1$. By antisymmetry with respect to the $z$-axis, we have $\partial_z p_D^+(x^1) = -\partial_z p_C^+(x^1)$. Because $p_D^-(x^1)$ only describes upgoing wavefields, we expect the quasi-horizontally propagating direct wave to be absent from $R_1^L(x^1, x_l^1)$ after practical implementation of this step.

## Derivation of the downward-radiating source Green's function matrix $G^+$

This matrix represents the surface response at $S_0$ for a virtual downward-radiating source at the new datum $S_1$. We apply the reciprocity theorem (equation A-5) to wave states $A$ and $B$ to obtain

$$
\begin{aligned}
\int_{S_1} \frac{2}{\rho(x^1)} g^{p,+}(x_i^0, x^1)\partial_z T^U(x^1, x_j^0)\mathrm{d}x^1 \\
= R(x_i^0, x_j^0) - R^U(x_i^0, x_j^0),
\end{aligned}
\tag{B-5}
$$

using the reciprocity relation $R(x_i^0, x_j^0) = R(x_j^0, x_i^0)$. A discretized version of this equation can be written as the matrix relation:

$$
\mathbf{G^+T^U} = \mathbf{R} - \mathbf{R^U}, \tag{B-6}
$$

where the matrices $\mathbf{R}$, $\mathbf{R^U}$, $\mathbf{T^U}$, and $\mathbf{G^+}$ are defined as

$$
\begin{aligned}
\{R\}_{ij} &= R(x_i^0, x_j^0), \\
\{R^U\}_{ij} &= R^U(x_i^0, x_j^0), \\
\{T^U\}_{ij} &= \partial_z T^U(x_i^1, x_j^0), \\
\{G^+\}_{ij} &= 2\Delta x g^{p,+}(x_i^0, x_j^1)/\rho(x_j^1).
\end{aligned}
\tag{B-7}
$$

We remind here that the boundary $S_0$ can be curvilinear and that the acquisition spatial interval along $x^0$ can be irregular.

## Derivation of the upward-radiating source Green's function matrix $G^-$

This matrix represents the surface response at $S_0$ for a virtual upward-radiating source at the new datum $S_1$. We apply the reciprocity theorem (equation A-5) to wave states $A$ and $C$, to obtain

$$
\begin{aligned}
&- g^{p,-}(x_i^0, x_k^1) + \int_{S_1} \frac{2}{\rho(x^1)} g^{p,+}(x_i^0, x^1)\partial_z R_1^U(x^1, x_k^1)\mathrm{d}x^1 \\
&= -T_1^U(x_i^0, x_k^1),
\end{aligned}
\tag{B-8}
$$

using the fact that $f_C = 0$ in the integration volume $V$. A discretized version of this equation can be written as the matrix relation:

$$
\mathbf{G^-} = \mathbf{T_1^U} + \mathbf{G^+R_1^U}, \tag{B-9}
$$

where the matrices $\mathbf{R_1^U}$, $\mathbf{T_1^U}$, and $\mathbf{G^-}$ are defined as

$$
\begin{aligned}
\{R_1^U\}_{ij} &= \partial_z R_1^U(x_i^1, x_j^1), \\
\{T_1^U\}_{ij} &= T_1^U(x_i^0, x_j^1), \\
\{G^-\}_{ij} &= g^{p,-}(x_i^0, x_j^1).
\end{aligned}
\tag{B-10}
$$

## Derivation of the redatumed reflection response $\mathbf{R_1^L}$

This matrix contains the redatumed data set that simulates an acquisition made at $S_1$ and for which the imprint of the overburden is completely removed. We apply the one-way reciprocity theorem (equation A-9) to wave states $A$ and $D$, and we choose a virtual boundary $S_2$ to be below the deepest reflector of the target area. Because there is no upgoing energy at this boundary, the one-way reciprocity theorem (equation A-9) simplifies to

$$
\int_{S_1} \frac{1}{\rho(x^1)} [p_A^+(x^1)\partial_z p_D^-(x^1) + p_A^-(x^1)\partial_z p_D^+(x^1)]\mathrm{d}x^1 = 0.
\tag{B-11}
$$

We replace the expressions of $\partial_z p_D^+$, $\partial_z p_D^-$, $p_A^+$, and $p_A^-$ to obtain

$$
\int_{S_1} \frac{1}{\rho(x_1)} g^{p,-}(x_i^0, x^1)\partial_z R_1^L(x^1, x_l^1)\mathrm{d}x_1 = -\frac{1}{2} g^{p,+}(x_i^0, x_l^1).
\tag{B-12}
$$

A discretized version of this equation can be written as the matrix relation:

$$
\mathbf{G^+} = \mathbf{G^-R_1^L}, \tag{B-13}
$$

where the matrix $\mathbf{R_1^L}$ is defined as

$$\{R_1^L\}_{ij} = -4(\Delta x)^2 \frac{\partial_z R_1^L(x_i^1, x_j^1)}{\rho(x_i^1)\rho(x_j^1)}. \qquad \text{(B-14)}$$

Note that $\Delta x$ appears squared to compensate for its presence in the definition of $\mathbf{G}^+$.

## REFERENCES

Aubry, J.-F., M. Tanter, J. Gerber, J.-L. Thomas, and M. Fink, 2001, Optimal focusing by spatio-temporal inverse filter. II. Experiments. Application to focusing through absorbing and reverberating media: The Journal of the Acoustical Society of America, **110**, 48–58, doi: 10.1121/1.1377052.

Bakulin, A., and R. Calvert, 2005, Virtual source: New method for imaging and 4D below complex overburden: 75th Annual International Meeting, SEG, Expanded Abstracts, 2477–2480.

Berryhill, J. R., 1979, Wave-equation datuming: Geophysics, **44**, 1329–1344, doi: 10.1190/1.1441010.

Broggini, F., R. Snieder, and K. Wapenaar, 2014, Data-driven wavefield focusing and imaging with multidimensional deconvolution: Numerical examples from reflection data with internal multiples: Geophysics, **79**, no. 3, WA107–WA115, doi: 10.1190/geo2013-0307.1.

da Costa Filho, C. A., M. Ravasi, A. Curtis, and G. A. Meles, 2014, Elastodynamic green's function retrieval through single-sided marchenko inverse scattering: Physical Review E, **90**, 063201, doi: 10.1103/PhysRevE.90.063201.

Hileman, J., P. Embree, and J. Pflueger, 1968, Automated static corrections: Geophysical Prospecting, **16**, 326–358, doi: 10.1111/j.1365-2478.1968.tb01980.x.

Minato, S., T. Matsuoka, and T. Tsuji, 2013, Singular-value decomposition analysis of source illumination in seismic interferometry by multidimensional deconvolution: Geophysics, **78**, no. 3, Q25–Q34, doi: 10.1190/geo2012-0245.1.

Mulder, W. A., 2005, Rigorous redatuming: Geophysical Journal International, **161**, 401–415, doi: 10.1111/j.1365-246X.2005.02615.x.

Ravasi, M., 2017, All-in-one marchenko redatuming: 79th Annual International Conference and Exhibition, EAGE, Extended Abstracts, doi: 10.3997/2214-4609.201701129.

Rayleigh, J. W. S., 1878, The theory of sound: MacMillan and Co.

Rose, J. H., 2002, Single-sided autofocusing of sound in layered materials: Inverse Problems, **18**, 1923–1934, doi: 10.1088/0266-5611/18/6/329.

Rothman, D. H., 1986, Automatic estimation of large residual statics corrections: Geophysics, **51**, 332–346, doi: 10.1190/1.1442092.

Schuster, G. T., and M. Zhou, 2006, A theoretical overview of model-based and correlation-based redatuming methods: Geophysics, **71**, no. 4, SI103–SI110, doi: 10.1190/1.2208967.

Shtivelman, V., and A. Canning, 1988, Datum correction by wave-equation extrapolation: Geophysics, **53**, 1311–1322, doi: 10.1190/1.1442409.

Singh, S., and R. Snieder, 2017, Strategies for imaging with Marchenko-retrieved greens functions: Geophysics, **82**, no. 4, Q23–Q37, doi: 10.1190/geo2016-0293.1.

Singh, S., R. Snieder, J. Behura, J. van der Neut, K. Wapenaar, and E. Slob, 2015, Marchenko imaging: Imaging with primaries, internal multiples, and free-surface multiples: Geophysics, **80**, no. 5, S165–S174, doi: 10.1190/geo2014-0494.1.

Slob, E., and K. Wapenaar, 2017, Theory for Marchenko imaging of marine seismic data with free surface multiple elimination: 79th Annual International Conference and Exhibition, EAGE, Extended Abstracts, doi: 10.3997/2214-4609.201700800.

Snieder, R., and K. vanWijk, 2015, A guided tour of mathematical methods for the physical sciences, 3rd ed.: Cambridge University Press.

Taner, M. T., F. Koehler, and K. Alhilali, 1974, Estimation and correction of near-surface time anomalies: Geophysics, **39**, 441–463, doi: 10.1190/1.1440441.

Tanter, M., J.-F. Aubry, J. Gerber, J.-L. Thomas, and M. Fink, 2001, Optimal focusing by spatio-temporal inverse filter. I. Basic principles: The Journal of the Acoustical Society of America, **110**, 37–47, doi: 10.1121/1.1377051.

Thorbecke, J. W., and D. Draganov, 2011, Finite-difference modeling experiments for seismic interferometry: Geophysics, **76**, no. 6, H1–H18, doi: 10.1190/geo2010-0039.1.

van der Neut, J., M. Tatanova, J. Thorbecke, E. Slob, and K. Wapenaar, 2011a, Deghosting, demultiple, and deblurring in controlled-source seismic interferometry: International Journal of Geophysics, **2011**, 870819, doi: 10.1155/2011/870819.

van der Neut, J., J. Thorbecke, K. Mehta, E. Slob, and K. Wapenaar, 2011b, Controlled source interferometric redatuming by crosscorrelation and multidimensional deconvolution in elastic media: Geophysics, **76**, no. 4, SA63–SA76, doi: 10.1190/1.3580633.

van der Neut, J., K. Wapenaar, J. Thorbecke, E. Slob, and I. Vasconcelos, 2015, An illustration of adaptive Marchenko imaging: The Leading Edge, **34**, 818–822, doi: 10.1190/tle34070818.1.

Vasconcelos, I., and J. van der Neut, 2016, Full-wavefield redatuming of perturbed fields with the Marchenko method: 78th Annual International Conference and Exhibition, EAGE, Extended Abstracts, doi: 10.3997/2214-4609.201600624.

Vasconcelos, I., K. Wapenaar, J. van der Neut, C. Thomson, and M. Ravasi, 2015, Using inverse transmission matrices for Marchenko redatuming in highly complex media: 85th Annual International Meeting, SEG, Expanded Abstracts, 5081–5086.

Wapenaar, C., and A. Berkhout, 1989, Elastic wave field extrapolation: Redatuming of single- and multi-component seismic data: Elsevier, Advances in exploration geophysics.

Wapenaar, C. P. A., and J. L. T. Grimbergen, 1996, Reciprocity theorems for one-way wavefields: Geophysical Journal International, **127**, 169–177, doi: 10.1111/j.1365-246X.1996.tb01542.x.

Wapenaar, K., 2014, Single-sided Marchenko focusing of compressional and shear waves: Physical Review E, **90**, 063202, doi: 10.1103/PhysRevE.90.063202.

Wapenaar, K., F. Broggini, E. Slob, and R. Snieder, 2013, Three-dimensional single-sided Marchenko inverse scattering, data-driven focusing, greens function retrieval, and their mutual relations: Physical Review Letters, **110**, 084301, doi: 10.1103/PhysRevLett.110.084301.

Wapenaar, K., E. Slob, and R. Snieder, 2008, Seismic and electromagnetic controlled-source interferometry in dissipative media: Geophysical Prospecting, **56**, 419–434, doi: 10.1111/j.1365-2478.2007.00686.x.

Wapenaar, K., J. Thorbecke, J. van der Neut, F. Broggini, E. Slob, and R. Snieder, 2014, Green's function retrieval from reflection data, in absence of a receiver at the virtual source position: The Journal of the Acoustical Society of America, **135**, 2847–2861, doi: 10.1121/1.4869083.

Wapenaar, K., and J. van der Neut, 2010, A representation for greens function retrieval by multidimensional deconvolution: The Journal of the Acoustical Society of America, **128**, EL366–EL371, doi: 10.1121/1.3509797.

Zhang, L., E. Slob, J. Van der Neut, and C. Wapenaar, 2016, Electromagnetic Marchenko imaging in 1d for dissipative media: 86th Annual International Meeting, SEG, Expanded Abstracts, 2479–2483.